J. Mater. Environ. Sci. 7 (3) (2016) 808-819
ISSN : 2028-2508
CODEN: JMESCN

Polyacrylamide-clay microcomposite as corrosion inhibitor for mild steel in 1m hydrochloric acid solution

Asma Mansri [1], Abdelaziz Bendraoua [1] and Brahim Bouras*[2]

[1]*Laboratoire de Synthèse organique, Physico-chimie, Biomolécules et Environnement (LSPBE) ; Département de Chimie Industrielle,Faculté des Sciences ; Université des Sciences et de la Technologie d'Oran- Mohamed Boudiaf-B.P1505 El'Mnaouer, Oran,31000, Algérie.*
[2]*Laboratoire d'Application des Electrolytes et des Polyélectrolytes Organiques (LAEPO). Département de Chimie. B. P. 119 13000 Tlemcen, Université de Tlemcen. Algeria.*

Received 26 Sep 2015, Revised 01 Dec 2015, Accepted 13 Dec 2015
**Corresponding author. E-mail: Bourasbrahim_m8@yahoo.fr Tel.: (+ 213 663415152)*

Abstract
The corrosion inhibition performance of mild steel in molar hydrochloric acid (1M HCl) solution in the presence of micro-composite [BC/PAM] (bleaching clay (Bentonite)) and polyacrylamide (synthetic polymer) was studied using weight loss and potentiodynamic measurements. The micro-composite reduces the corrosion rate and the inhibition efficiency (E_W%) of BC/PAM increases with its concentration and attains 80% at 400 mg/l. E_W% obtained from cathodic Tafel plots, electrochemical impedance spectroscopy (*EIS)* and gravimetric methods were in good agreement. The various thermodynamic parameters of metal dissolution and micro-composite adsorption process were elaborated by the adsorption mechanism. Adsorption of the inhibitor obeyed to Freundlich adsorption isotherm.

Keywords: Polyacrylamide (PAM), Bleaching Clay (BC), Micro-composite, Corrosion, Mild Steel.

1. Introduction
Corrosion of metals is a major problem that must be confronted for safety, environment and economic reasons [1]. Mild steel is an important material of choice due to low cost and easy availability. Acids are deployed in many service environments such as pickling, cleaning of boilers, des-scaling and acidification of oil well. Unfortunately, the acid tends to induce corrosion which, if not checked, could reduce the service life of the metal [2]. Inhibitors are added to such acid solution in order to reduce the degree of metal attack and the rate of acid consumption [3–5]. The use of some chemical inhibitors have been limited because of some reasons namely their synthesis is very often expensive and they can be toxic and hazardous for human beings environment as well [6].

Inorganic substances are effective acid corrosion inhibitors but their uses have been discouraged because of environmental issues [5, 6]. Most of the efficient inhibitors are organic compounds that contain in their structures mostly nitrogen, sulfur or oxygen atoms [6-10]. The results show that the inhibitory efficiency increases with inhibitor concentrations. Therefore, they minimize the direct interaction between the metal and corrosive agents. In some cases, the coordination of the inhibitor molecules to the surface is weak, and their presence in the corrosive solutions required maintaining the desired concentration of these agents to the metal surface [10–16]. It has been observed that adsorption depends mainly on certain physico-chemical properties of the inhibitor group, such as functional groups, electron density at the donor atom, π-orbital character and the electronic structure of the molecule [17]. Recently, the use of polymers as corrosion inhibitors have drawn considerable attention due to their inherent stability, low prices of polymers, availability and cost effectiveness. More so, through their functional groups, they form complexes with metal ions and on the metal surface. These complexes occupy a large surface area by blanketing this later and protecting the metals from corrosive agents present in the solution [18]. Some recent reports on the use of polymers as corrosion inhibitors of metals in

aggressive media can be found in the literature. Polymers such as Poly(acrylamide), poly(acrylic acid), poly(4-vinylpyridine), poly(4-vinylpyridine isopentylbromide), poly(4-vinylpyridine poly-3-oxide ethylene) and poly(acrylamide-co-4vinylpyridine) have been reported [18–20].

Polymer/clay nano-composites (PCN) are now of great interest to polymer scientists, physicists and material scientists because of the unique properties produced by combining these components at the nanoscale level. Measuring the corrosion protection effects of PCN as coatings is crucial to gaining a fundamental understanding of the anticorrosion mechanism of these materials.

Measurement of the anticorrosive properties of PCN is also helpful in establishing the gas barrier properties of polymer/clay interactions and their structure-property relationship in nano-composites. This is because anticorrosive performance is strongly influenced by the nanoscale structure and interfacial characteristics [21]. The present work reports on the corrosion inhibition efficiency of one micro-composite newly synthesized on mild steel in 1M HCl solution at 25 °C using chemical and electrochemical techniques.

2. Materials and methods

2.1. Materials

A sample of Bentonite (BC) was supplied by a local company (ENOF). It was obtained from industrial treatment of natural clay issued from the fields of Hammam Boughrara–Maghnia, Algeria. It is composed essentially of montmorillonite [22-24]. The different chemical elements of the bentonite (Table 1) were transformed into oxides and analyzed by X-ray fluorescence at the (ENOF) central laboratory. The results are given in Table 1, confirming that the bentonite consists essentially of montmorillonite, since the SiO_2/Al_2O_3 ratio is equal to 3.77, and belongs to the family of the phyllosilicates [22-24]. In addition, as expected, this bentonite forms stable suspensions in water and has flat-plate or needle-like structures. Granulometry of the crude bentonite was performed locally in the Civil Engineering Department (Tlemcen University) using a sedimentation technique with 0.1 % solution of sodium hexametaphosphate. It was found that 95 % of the grains had diameter inferior to 100 µm. The cation exchange capacity (CEC) was 80 meq/ 100 g of clay. The surface area was $27 m^2/g$ with pore size average of 7 nm [25-27].

The reagents used are acrylamide monomer (AM), ammonium persulfate (APS) as free-radical initiator and surfactant N-dodecylpyridinium chloride (DPC). They were supplied by the Aldrich Company. The only solvent used was bidistilled water.

Table 1: Chemical composition of the Bentonite BC.

Species	**SiO_2**	**Al_2O_3**	**Fe_2O_3**	**CaO**	**MgO**	**Na_2O**	**K_2O**	**TiO_2**	**LOI**
% (w/w)	65.2	17.25	2.10	1.20	3.10	2.15	0.60	0.20	8.20

2.2. Synthesis and characterization of the micro-composite

[PAM/BC] micro-composite was synthesized by (AM) in-situ polymerization [26-28]. In a 500ml round flask, 10g of Bentonite (BC) were dispersed in 200ml of bidistilled water. Introduce 4g of DPC surfactant and mix strongly the dispersion under nitrogen atmosphere for 120 min. 1g of the APS initiator was added to the mixture and stirred for 30 min. Finally, 20g of the monomer acrylamide (AM) was added to the mixture. The sample was polymerized in an oil bath at 80°C for 12 h to obtain the micro-composite **[PAM/BC]**. The obtained micro-composite **[PAM/BC]** was dispersed in ethanol, filtered and dried under vacuum.The micro-composite was characterized by FTIR using a Perkin-Elmer-2000 spectrophotometer with samples in the form of KBr pellets. The obtained results are given in Table 2.

Table 2: FTIR spectrum of micro-composite

Frequency υ (cm^{-1})	**Attribution**	**Nature**
3168-3331	N-H	Elongation vibration
2928	C-H	Elongation vibration
1600-1750	C=O	Elongation
1413	C-N	Elongation

Indeed, the thermo gravimetric (TGA) experiments were carried out on a TGA V5.2E Instruments 2950 analyzer. Measurements were performed under air atmosphere. Same conditions were used for all tests, with a

heating rate of 10°C/min in the temperature range between 0 to 1000°C under air flow. Table 3 regroups the results of this characterization.

Table 3: [PAM/BC] micro-composite weight percentage composition

Sample	Initial rate AM (g)	Initial rate BC (g)	Weight loss from 20 to 400 °C	Weight loss from 400 to 900 °C	Final rate of AM (%)
BC (clay)	//	//	4.5-4.6	00.00	00
PAM	5	00.00	80%	≈ 100%	100
Micro-composite	5	5	18.74	39.98	**54.12**

Finally, the Differential Scanning Calorimetry (DSC) was realised by a Perkin-Elmer DSC-7 differential scanning calorimeter, to measure the glass transition temperature Tg of the samples (calibration with indium and heating rate of 10°C min^{-1}. Tg was taken as the midpoint of the step change in the heat flow. The glass transition temperature (Tg) of pure PAM [29] is 161 °C while the Tg of the micro-composite is Tg=195,1 °C. It is higher than that of the pure PAM. We observe a great increasing of the Tg transition temperature, which is due to the incorporation of the PAM onto the Bentonite, and where the polymer is confined in the interlayer space and could not move freely.

2.3. Samples and materials

Prior to each gravimetric or electrochemical experiment, the surface of the specimens was abraded successively with emery paper. The samples were polished finally with emery paper up 1200 grade. Weight loss was measured on sheets of steel of 2 cm^2 apparent surface area. The specimens were then rinsed with acetone and bi-distilled water before being weighed and immersed in 50 ml of the corrosive medium. A clean weighed mild steel sample was completely immersed at an inclined position in the vessel for 2 h of immersion in 1M HCl, with and without the addition of inhibitor at different concentrations.
A solution of 1M HCl was prepared from an analytical reagent grade 37 % HCl and bi-distilled water and was used as corrosion media. The chemical composition of mild steel is given in Table 4.

Table 4: The chemical composition of mild steel

% C	% Mn	% P	% S	% Cr	% Nor	% Mo	% V	% Cu	% Al	%Fe
0.199	1.59	0.016	0.018	0.015	0.007	0.008	0.004	0.024	0.024	Balance

Electrochemical measurements were carried out in a conventional three-electrode electrolysis cylindrical Pyrex glass cell. The working electrode had the form of a disc cut form steel sheet. The exposed area to the corrosive solution was 1 cm^2. A saturated calomel electrode (SCE) and a platinum electrode were used, respectively as a reference and auxiliary electrodes. All potentials are given in the SCE scale. The cell is thermostated at 291 ±1 K. The current–voltage curves are recorded with a potentiostat (Amel 549) using a linear sweep generator (Amel 567) at a scan rate of 1V/min. Before recording the cathodic curves, the iron electrode was polarised at 800 mV for 10 min. For anodic curves, the potential of the electrode was swept from its open circuit value after 30 min free corrosion. The test solution was de-aerated for 30 min in the cell with pure nitrogen. Gas bubbling was maintained throughout the experiments.
Electrochemical impedance spectroscopy (EIS) was carried out with a voltalab PGZ 100 electrochemical system at E_{corr} after immersion in solution. After determination of the steady-state current at a given potential, sine wave voltage (10 mV) peak to peak, at frequencies between 100 kHz and 10 mHz, was superimposed on the rest potential. Computer programs automatically controls the measurements performed at rest potentials after 30 min of exposure. EIS diagrams are given in the Nyquist representation.

3. Results and discussions

3.1. Weight loss measurements

The effect of addition of micro-composite **[PAM/BC]** tested at different concentrations on the corrosion of steel in 1M HCl solution was studied by weight loss at 25°C after 2 h of immersion. Inhibition efficiency (Ew %) is calculated as follows Eq. (1):

$$E_w\% = \left(1 - \frac{W_{corr}}{W^o_{corr}}\right).100 \quad (1)$$

Where $W°_{corr}$ and W_{corr} are the corrosion rates of iron samples in the absence and presence of the inhibitor, respectively.

The Values of corrosion rate and inhibition efficiencies are given in Table 5. The results of weight loss study showed that the addition of the micro-composite reduces the corrosion rate in HCl 1 M solution. The inhibition efficiency increases with increasing inhibitor (micro-composite) concentrations. The optimum concentration of inhibitor required to achieve an efficiency of 79.3 % is found to be 400 mg l^{-1}. The inhibition by the micro-composite can be explained in terms of adsorption on the metal surface.This adsorption of the micro-composite molecules could occur due to the formation of links between the d-orbital of iron atoms, involving the displacement of water molecules from the metal surface, and the lone electron pairs present on the N and O atoms. It is shown that the compounds, having a higher electron density load around the heteroatoms, exhibit protective properties which depend upon their ability to reduce the corrosion rate.

Table 5: Inhibition efficiency for corrosion of mild steel in 1M HCl with different concentrations of micro-composite obtained from weight loss measurements at 25°C.

Inhibitor	Concentration (mg/l)	W (mg cm^{-2} h^{-1})	E_W (%)
1M HCl	-	0.27708	-
Micro-composite [PAM/BC]	5	0.23381	15.6
	10	0.21875	21.1
	50	0.19270	30.5
	100	0.18229	34.2
	200	0.13437	51.5
	300	0.09427	66.5
	400	0.05729	79.3

The micro-composite compound containing electron negative function groups and π electrons conjugated are usually good inhibitors [9-15, 30-35]. The compound can be absorbed by the interaction between the lone pair of electrons of the nitrogen and oxygen atoms and the metal surface

3.2. Influence of temperature

In order to study the effect of temperature on corrosion inhibition of mild steel in acid during a period of two hours and at different concentrations and to determine the activation energy for the corrosion process, the weight loss studies were carried out at various temperatures (298–353 K) without and with the micro-composite. The corresponding results are given in Table 6.

Table 6: Variation of inhibition efficiency's according to temperature.

Temperature (K)	E_W (%) at 400mg/l	E_W (%) at 300mg/l	E_W (%) at 200mg/l	E_W (%) at 100mg/l	E_W (%) at 50mg/l
298	79.32	66.54	51.50	34.21	30.45
313	88.49	74.24	57.53	38.21	34.01
333	93.58	89.45	69.32	46.04	40.97
353	97.06	94.37	73.13	48.57	43.23

From these results in Table 6, it is clear that the inhibition efficiency increases with increasing temperature. Figure 1 gives the variation of the inhibition efficiency's according to the temperature.

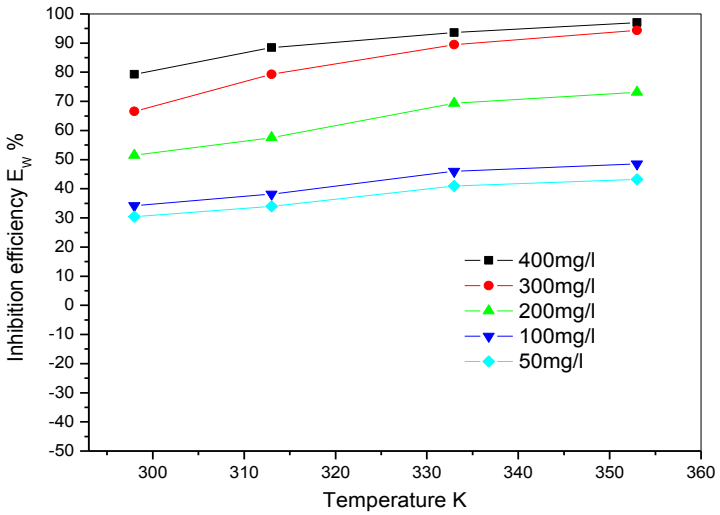

Figure 1: Variation of the inhibition efficiency's according to the temperature.

We can deduce that the corrosion rate increases in the blank with the rise of temperature, but in the presence of the micro-composite, the dissolution of mild steel is widely retarded. The values of inhibition efficiency obtained from the weight loss at various temperatures show that the inhibition efficiency increases with increasing temperature indicating that higher temperature favours the adsorption of composite on the dissolution of steel at the surface. The corrosion process and protectiveness of an inhibitor are significantly dependent on the temperature. We may conclude that micro-composite is an excellent inhibitor of iron corrosion in 1M HCl solution at high temperature. E_W% reaches a maximum of 97% at 400 mg/l for micro-composite.

3.3. Thermodynamic parameters

Thermodynamic parameters such as activation energy Ea, enthalpy and entropy of micro-composite were calculated using Arrhenius plot (the logarithm of steel corrosion rate vs.1000/T, Fig. 2) for the corrosion rate for both the blank and micro-composite solution.

From this relation (2), we can determine the apparent activation energies:

$$\log(W_{corr}) = \frac{-E_a}{RT} + A \qquad \text{and} \qquad \log(W'_{corr}) = \frac{-E_a'}{RT} + A \qquad (2)$$

E_a and E_a' are the apparent activation energies with and without the micro-composite, respectively. T is the absolute temperature, A is a constant and R is universal gas constant.

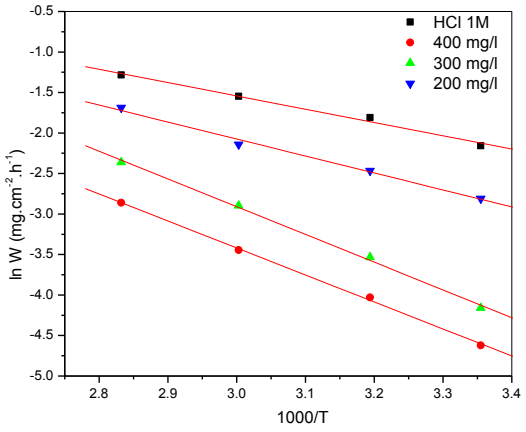

Figure 2: Arrhenius plots of the corrosion rate for both the blank and the solution of micro-composite

It can be seen that the corrosion weight loss for mild steel increases more rapidly with temperature in uninhibited solution than in inhibited solution. This result confirms that inhibitor act as an efficient corrosion inhibitor in the range of temperature studied.

Kinetic parameters, such as enthalpy and entropy of corrosion process, may be evaluated from the effect of temperature by an alternative formulation of transition state equation (Eq.3) [36].

$$W = \frac{RT}{N.h}\exp\left(\frac{\Delta S^{0}{}_{a}}{R}\right)\exp\left(-\frac{\Delta H^{0}{}_{a}}{RT}\right) \qquad (3)$$

Where h is Plank's constant, N Avogadro number, $\Delta S°_a$ and $\Delta H°_a$ are, respectively, the entropy and enthalpy of activation.

Table 7 presents the calculated values of E_a, $\Delta S°_a$ and $\Delta H°_a$ in inhibited and uninhibited acid. It is observed that the activation energy is higher in the presence of micro-composite inhibitor than in its absence.

Table 7: Thermodynamic parameters at different concentrations of the micro-composite

***C* (mg/l) Polymer**	**E_a (kJ mole^{-1})**	**ΔH^* (kJ mole^{-1})**	**ΔS^* (J mole^{-1})**
HCl 1M	13.944	11.172	-26.609
200	14.505	11.735	-26.622
300	28.664	25.893	-27.497
400	31.071	28.307	-27.919

The value of activation energy (E_a) found is greater than that in the uninhibited solution. While the higher value of the activation energy of the process in an inhibitor's presence when compared to that in its absence is attributed to its physical adsorption. The physical adsorption is a result of electrostatic attraction between charged metal surface and charged species in the bulk of the solution. Adsorption of negatively charged species is facilitated if the metal surface is positively charged. Positively charged species can also protect the positively charged metal surface acting with a negatively charged intermediate, such as acid anions adsorbed on the metal surface [30-38].

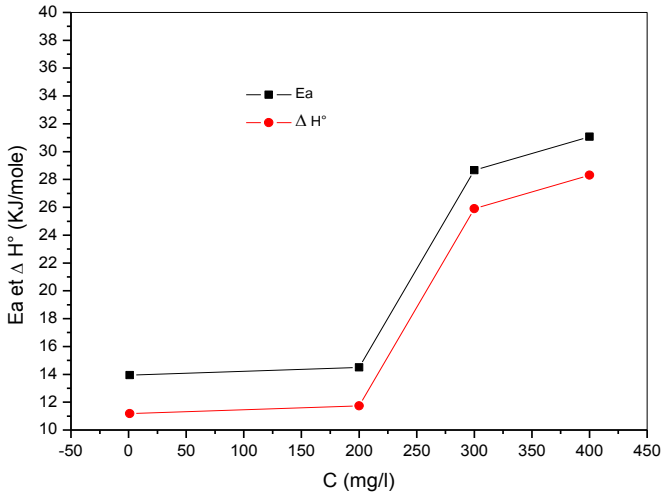

Figure 3: Variation of E_a and ΔH°_a according to the inhibitor concentrations.

The values of $\Delta H°_a$ are reported in Table 7. The heat of adsorption is known to be a good measure of the strength of adsorption on the surface. Thus, The positive sign of the enthalpy ($\Delta H°_a$) reflects the endothermic nature of the steel dissolution process and values vary in the same way with inhibitor concentration and acid solutions.

On the other hand, values of $\Delta S°_a$ are more positive in solutions acid containing inhibitors than those obtained in the uninhibited solutions. This behaviour can be explained as a result of the replacement process of water molecules during adsorption of inhibitors on steel surface. This observation is in agreement with the literature [37, 38]. However, the negative values of entropies imply that the activated complex in the rate-determining step represents an association rather than a dissociation step, meaning that a decrease in disordering takes place on going from reactants to the activated complex [6-11, 15-38]. One can notice that E_a and $\Delta H^{\circ}_{values}$ vary in the same way (Fig. 3). This result permits to verify the known thermodynamic reaction between the E_a and ΔH°_a as shown in Table 7.

$$\Delta H_a^0 = E_a - RT \qquad (4)$$

3.4. Adsorption isotherm

Adsorption isotherms are very important for the understanding of the mechanism of orgango-electrochemical reaction. The most frequently used isotherms are Langmuir, Freundlich, etc. [7-8, 15, 37].

Several adsorption isotherms were assessed and the Freundlich adsorption isotherm was found to be the best description of the adsorption behaviour of the studied inhibitor. Using Freundlich isotherm as model, the quantities Adsorbed are related by equation (Eq. 5)

$$\theta = K_N C^{\frac{1}{n}}$$

$$Ln\theta = LnK_N + \frac{1}{n} LnC \qquad (5)$$

Where K_N is the Freundlich constant which represents the capacity of the adsorbent, n heterogeneity factor, C the inhibitor concentration and θ the fraction of the surface covered determined by $E_w/100$.

$\Delta G°_{ads}$ the standard free energy of adsorption is calculated using the equation of Gibbs Helmholtz (Eq.6).

$$\Delta G^0 = -RTLnK_N \qquad (6)$$

Figure 4 shows the dependence of the ratio θ as function of inhibitor concentration (C) and Lnθ as function of LnC at different temperature. Taking the second case, the obtained plot is linear with a slope 0.6. The regression coefficient is r = 0.981. The intercept permit the calculation of the Freundlich constant K_N.

This result leads to evaluating ΔG° = - 6.4 kJ/mol. this value indicates that inhibitor interacts on the steel surface by electrostatic effect. We note also in Table 8, that the negative values of $\Delta G°_{ads}$ ensure and confirmed the spontaneity of the adsorption process and stability of the adsorbed layer on the steel surface [5, 8, 38] and the lower are consistent with the electrostatic interaction between the charged molecules and the charged metal and confirmed that the adsorption is physi-sorption. The negative values of $\Delta G°_{ads}$ suggest that the adsorption of the inhibitor onto the steel surface follows a spontaneous process. The result is confirmed by Gibbs Helmholtz and thermodynamic calculations. The obtained values of ΔG^{o}_{ads} show the regular dependence of ΔG^{o}_{ads} on temperature (Table 8), indicating a good correlation among thermodynamic parameters. However, a limited decrease in the absolute value of ΔG^{o}_{ads} with an increase in temperature it was observed. This behaviour is explained by the fact that the adsorption is somewhat unfavourable with increasing experimental temperature, indicating that the physisorption has the major contribution while the chemisorptions has the minor contribution in the inhibition mechanism [5, 8, 37-38].

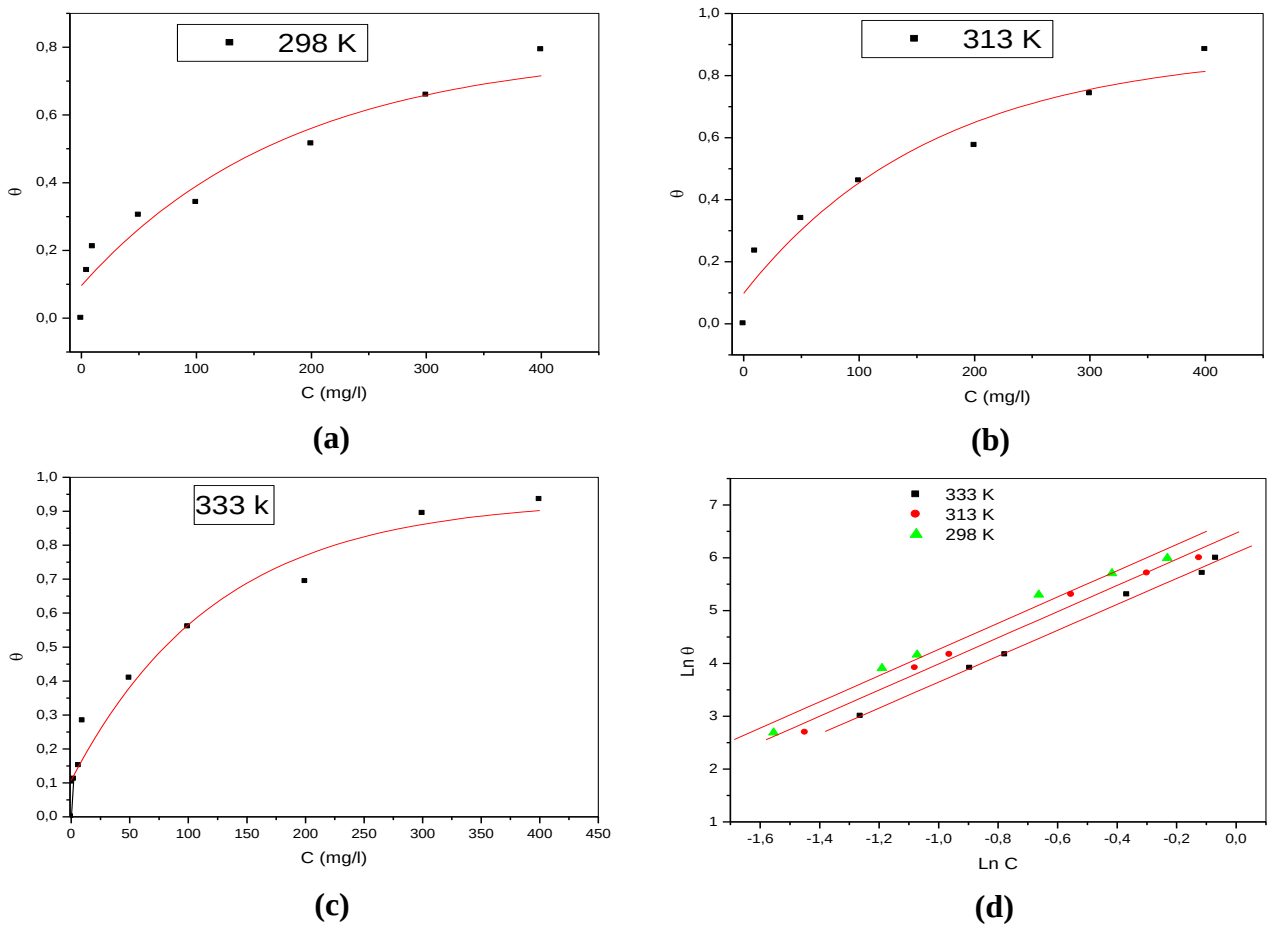

Figure 4: Freundlich adsorption isotherm
Plots of **(a)**, **(b)** and **(c)** are for θ Vs. inhibitor concentration (C) indeed plot **(d)** ln (θ) Vs. (ln C) for the corrosion of steel in 1M HCl solution

Table 8: Adsorption thermodynamic parameters of steel inhibitor at different temperatures

Temperature (K)	**n**	**K_N ($mg^{1-(1/n)}L^{1/n}g^{-1}$)**	**linear regression coefficient (r)**	**ΔG°_{ads} ($kJ\ mole^{-1}$)**
298	1.67	11.58	0.992	-6.1
313	1.65	11.82	0.997	-6.4
333	1.66	11.94	0.991	-6.8

3.5. Polarisation measurements

Current–potential characteristics resulting from cathodic and anodic polarisation curves of steel in 1M HCl in presence of the micro-composite at various concentrations are evaluated. The cathodic Tafel

plots of micro-composite are shown in Fig.5, Table. 9, collects electrochemical parameters and inhibition efficiencies (E_I) which are determined by equation (Eq.7):

$$E_I\% = \left(1 - \frac{I_{corr}}{I^o_{corr}}\right).100 \qquad (7)$$

I_{corr} and I°_{corr} are the corrosion current density values with and without the inhibitor, respectively, determined by extrapolation of cathodic Tafel lines to the corrosion potential.

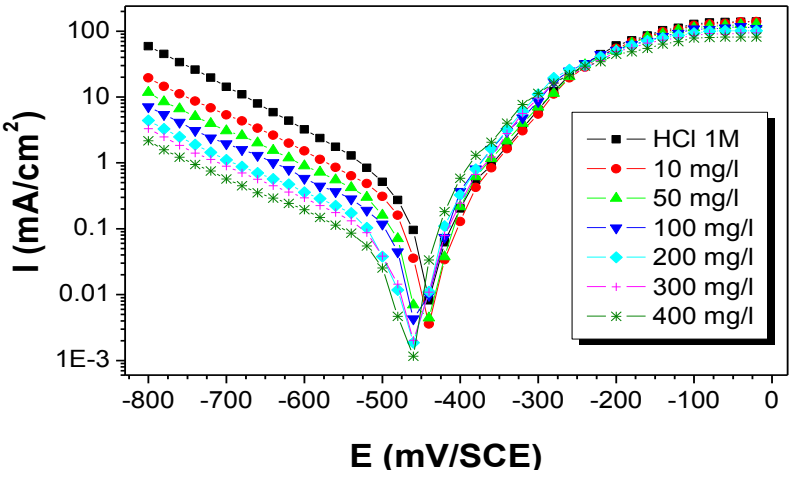

Figure 5: Cathodic and anodic polarisation curves of mild steel in 1M HCl at different concentrations of micro-composite

Table 9: Polarization parameters and corresponding inhibition efficiencies of mild steel corrosion in 1M HCl containing different concentrations of micro-composite at 298 K

Inhibitor	**Concentration (mg/l)**	**E_{corr} (mV/SCE)**	**β_c (mV/dec)**	**I_{corr} ($\mu A/cm^2$)**	**E_I (%)**
Blanc	HCl 1M	-445	152	305	-
Micro-composite	10	-444	178	244	20
	50	-448	183	213	30
	100	-451	187	207	32
	200	-455	189	152	50
	300	-456	191	104	66
	400	-458	187	67	78

From results obtained in the Table 9, a decrease of corrosion current densities was noted when the concentration of the inhibitor increases. The inhibiting action is more pronounced with inhibitor and their inhibition efficiency attains a maximum value of 78%, respectively, at 400mg/l. The obtained parallel Tafel curves indicate that hydrogen evolution reaction is activation controlled and the addition of the micro-composite does not modify the mechanism of this process [11].

In the presence of the micro-composite, the anodic curves show that the molecules effect depends on the electrode potential. It seems that inhibitor compounds tested have no effect from the overvoltage higher than E_{corr}. The addition of the micro-composite shifted the E_{corr} value towards to negative direction. This indicates that they control compounds used predominantly cathodic reaction and act as cathodic inhibitors.

3.6. Electrochemical impedance spectroscopy (EIS)

To complete and to compare the results obtained before, the corrosion behaviour of mild steel, in chloride acid solution with and without inhibitors, was investigated by electrochemical impedance spectroscopy (*EIS*) at 298K after 30 min of immersion (Fig. 6). The charge-transfer resistance (R_t) values were calculated from the

difference in impedance at lower and higher frequencies [9, 39]. The double layer capacitance (C_{dl}) was obtained at the frequency f_m at which the imaginary component of the impedance is maximal ($Z_{i,max}$) by Eq. (8):

$$C_{dl} = \frac{1}{2\pi f_m . R_t} \quad (8)$$

The inhibition efficiency from the charge transfer- resistance was calculated by Eq. (9):

$$E_{R_t}(\%) = \frac{R_t^{'} - R_t}{R_t^{'}} \times 100 \quad (9)$$

Where R_t and R'_t are the charge transfer-resistance values with and without the inhibitor, respectively.

Typical Nyquist diagrams obtained in the presence of various concentrations of micro-composite are shown in Fig. 6. The deduced impedance parameters as transfer resistance R_t (Ω cm^2), double-layer capacitance C_{dl} (μF/cm^2) and corresponding inhibition efficiency (E_{Rt} %) are shown in Table 10.

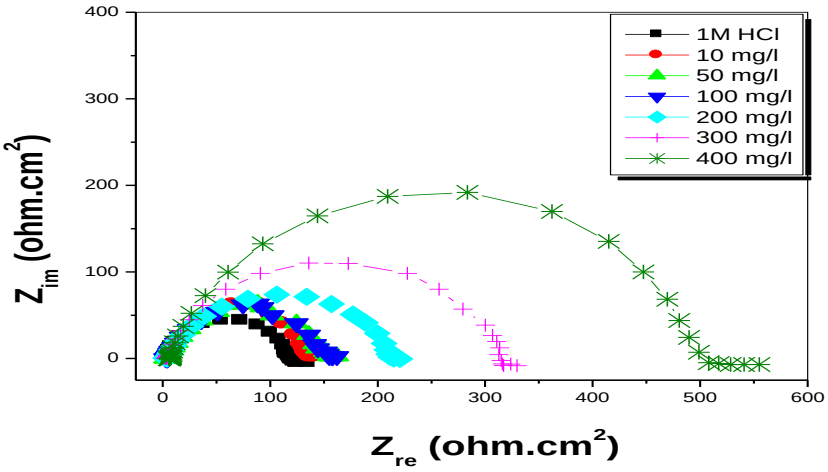

Figure 6: Nyquist plots for mild steel in 1M HCl containing different concentrations of micro-composite

Table 10: Impedance parameters for corrosion of mild steel in 1M HCl with different concentrations of micro-composite

C(micro-composite) mg l^{-1}	R_t (Ω cm^2)	C_{dl} (μF cm^{-2})	E(%)
Blank	115	87.51	—
10	142	80.22	19
50	160	75.47	28
100	162	74.04	29
200	217	69.75	47
300	329	61.03	65
400	500	51.40	77

It is seen from Fig. 6 that the impedance diagrams show semi-circles. We remark that the increase of R_t and decrease of double-layer capacitance (C_{dl}) and the efficiency increases when the concentration of micro-composite increases.

The obtained impedance diagrams show almost a semi-circular appearance, indicating a charge transfer process mainly controls the corrosion of mild steel. In fact, the presence of micro-composite compound enhances the value of R_t in acidic solution. Values of double-layer capacitance are also brought down to the maximum extent in the presence of micro-composite and the decrease in the values of C_{dl} follows the order similar to that obtained for I_{corr} in this study. The decrease in C_{dl} may be due to the adsorption of this compound on the metal surface, leading to the formation of film from acidic solution [5, 20, 22, 40-41].

Conclusion

The micro-composite obtained from naturally clay (BC) and polyacrylamide (PAM) inhibits the corrosion of mild steel in molar hydrochlorid acid solution. A better performance about 80% is seen in the presence of 0,4g/l of the inhibitor. The adsorption of BC-PAM micro-composite inhibitor, on the steel surface in molar hydrochlorid acid solution, obeyed Freundlich adsorption isotherm.

The obtained results from the different weight loss, the electrochemical impedance spectroscopy and polarization curves are in reasonably good agreement.

The negative values of $\Delta G°_{ads}$ ensure and confirm the spontaneity of the adsorption process and stability of the adsorbed layer on the steel surface and suggest that the adsorption of the inhibitor onto the steel surface is a spontaneous process. The free energy values indicate also that the inhibitor interacts on the steel surface by an electrostatic effect.

References

1. Abed Y., Hammouti B., Touhami F., Aouniti A., Kertit S., Mansri A., Elkacemi K., *Bull. Electrochem.*, 17 (2001) 105.
2. Mansri A., Bouras B., *Mor. J. Chem.*, 2 (2014) 252.
3. Popova A., Sokolova E., Raicheva S., Christov M., *Corros. Sci*., 45 (2003) 33.
4. Noor E.A., Corros. Sci., 47 (2005) 33
5. Mansri A., Bouras B., Hammouti B., Warad I., Chetouani A., *Res. Chem. Intermed*., 10.1007/s11164-012-0547-4 (2012)
6. Li Y., Zhao P., Liang Q., Hou B., *Appl. Surf. Sci*., 252 (2005) 1245.
7. Fekry AM., Mohamed R.R., *Electrochim. Acta*., 55 (2010) 1933.
8. Umoren S.A., Li Y., Wang F.H., *Corros. Sci*., 53 (2011) 1778.
9. Bentiss F., Traisnel M., Lagrenee M., *Corros. Sci*., 42 (2000) 127.
10. Behpour M., Ghoreishi S.M., Mohammadi N., Salavati-Niasari M., *Corros. Sci*., 53 (2011) 3380.
11. Chetouani A., Hammouti B., Benhadda A.T., Daoudi M., *Appl. Surf. Sci*., 249 (2005) 375.
12. Laarej K., Bouachrine M., Radi S., Kertit S., Hammouti B., *Arab J. Chem*., 7 (2010) 419.
13. Barouni K., Bazzi L., Salghi R., Mihit M., Hammouti B., Albourine A., El Issami S., *Mater. Lett*., 62 (2008) 3325.
14. Zerfaoui M., Oudda H., Hammouti B., Kertit S., Benkaddour M., *Prog. Org. Coat*., 51 (2004) 134.
15. Amin M.A., Khaled K.F., Mohsen Q., Arida H.A., *Corros. Sci*., 52 (2010) 1684.
16. Bertrand N., Desgranges C., Poquillon D., Lafont M.C., Monceau D., *Oxid. Met*., 73 (2010) 139.
17. Emregül K.C., Hayvalı M., *Mater. Chem. Phys*., 83 (2004) 209.
18. Rajendran S., Sridevi S.P., Anthony N., John Amalraj A., Sundaravadivedi M., *Anti-corros. Methods Mater*., 52 (2005) 102.
19. Mansri A., Bouras B., Tennouga L., Medjahed K., *Der Pharm. Chem*., 4(5) (2012) 1803.
20. Umoren S.A., Lia Y., Wang F.H., *Corros. Sci*., 52 (2010) 1777.
21. Weng C.J., Chang C.H., Yeh J.M., *Corr. Prot. and Control Using nanomaterials*., (2012) 330.
22. Larabi L., Harek Y., Traisnel M., Mansri A., *J. Appl. Electrochem*., 34 (2004) 833.
23. Zhang B.Q., Chen G.D., Yuan Pan C., Luan B., Hong C.Y., *J. Appl. Polym. Sci*., 102 (2006) 1950.
24. Li N., He B., Xu S., Yuan J., Miao J., Niu L., Song J., *Mater. Chem. Phys*., 133 (2012) 726.
25. Mansri A., Ramdani N., *Res Chem Intermed*., 41 (2015) 1765.
26. Kalbasi R.J., Mosaddegh N., *Catal. Commun*., 12 (2011) 1231.
27. Changchaivong S., Khaodhiar S., *Appl. Clay Sci*., 43 (2009) 317.

28. Huskic M., Igon M.Z., *Eur. Polym. J*., 43 (2007) 4891.
29. Moulay S., Bensacia N., Garin F., Ioana F., *Anne Boos, C.R. Chimie.*, 17 (2014) 849.
30. Umoren S.A., Eduok U.M., Oguzie E.E., *Portgu. Electrochim. Acta*., 26 (2008) 533.
31. Bouanis F.Z., Jama C., Traisnel M., Bentiss F., *Corros. Sci*., 52 (2010) 3180.
32. Belkaid S., Tebbji K., Mansri A., Chetouani A., *Res Chem Intermed.*, 38 (2012) 2309.
33. Gesmundo F., Viani F., *Mater. Chem. Phys*., 20 (1988) 513.
34. Doner A., Solmaz R., Ozcan M., Kardas G., *Corros. Sci*., 53 (2011) 2902.
35. Bentiss F., Lagrenee M., Traisnel M., Mernari B., Elattari H., *J. Appl. Electrochem*., 29 (1999) 1073.
36. Bouanis F.Z., Jama C., Traisnel M., Bentiss F., *Corros. Sci*., 52 (2010) 3180.
37. Bouklah M., Attayibat A., Kertit S., Ramdani A., Hammouti B., *Appl. Surf. Sci*., 242 (2005) 399
38. Doner A., Kardas G., *Corros. Sci*., 53 (2011) 4223.
39. Umoren S.A., Ebenso E.E., *Mater. Chem. Phys*., 106 (2007) 387.
40. Chetouani A., Aouniti A., Hammouti B., Benchat N., Benhadda T., Kertit S., *Corros. Sci*., 45 (2003) 1675.
41. Chetouani A., Hammouti B., Aouniti A., Benchat N., Benhadda T., *Prog. Org. Coat*., 45 (2002) 373.